Accuracy of Point and Line Measures of Boundary Layer Cloud Amount

LARRY K. BERG AND ROLAND B. STULL

Atmospheric Science Programme, Department of Earth and Ocean Sciences, The University of British Columbia, Vancouver, British Columbia, Canada

(Manuscript received 29 January 2001, in final form 5 November 2001)

ABSTRACT

Many authors have used upward-looking instruments, such as a laser ceilometer, to estimate the cover of fair-weather cumuli, but little has been mentioned as to the accuracy of these measurements. Results are presented, using a simulated cloud field and a virtual aircraft, that show that sampling errors can be very large for averaging times commonly used with surface instruments. A set of empirical equations is found to provide an estimate of the errors associated with averaging time and earth cover. These relationships can be used to design observation strategies (averaging time or flight-leg length) that provide earth-cover estimates within desired error bounds. These results are used to guide a comparison between earth cover measured by an airborne upward-looking pyranometer and earth cover observed by airborne scientists in a research aircraft. In general, the agreement between these two methods is good.

1. Introduction and motivation

One of the oldest, and perhaps most common, methods of observing cloud cover is to use a human observer stationed on the ground. In this case, the observer reports the fraction of sky dome that is covered with clouds. As an alternative, cloud cover can be reported in terms of the fraction of the earth's surface that is covered by clouds. This value can be measured with a downward-looking satellite. It also can be measured as a cloud field is blown over a vertically looking, narrowbeam sensor on the ground or as a sensor on an aircraft is flown over or under a cloud field. These two measures of cloud amount are usually not the same, because both the cloud base and cloud sides block parts of the sky dome, so that sky cover is greater than earth cover (Appleman 1962; Hoyt 1977). Both Malick et al. (1979) and Henderson-Sellers and McGuffie (1990) have developed empirical relationships that couple these two kinds of observations.

These different definitions of cloud cover may be useful for different applications. The sky cover is useful for radiation budget measurements in which presence of cloud sides contributes to both the short- and longwave radiation received at a point on the surface. Earth cover of fair-weather cumuli is a pertinent parameter for coupling boundary layer processes to the amount of cloud cover and for determining the transfer of pollutants out of the convective boundary layer.

Many researchers, as well as the Automated Surface Observing System (ASOS) used by the National Weather Service and Federal Aviation Administration, use a ceilometer, lidar, or other vertically looking active sensor to estimate earth cover [Bretherton et al. (1995), White et al. (1995), Fairall et al. (1997), ASOS Program (1998), Grimsdell and Angevine (1998), and Lazarus et al. (2000) are recent examples]. For these instruments a cloud is detected when the sensor's emitted light is scattered off clouds and returned to a detector on the surface. Earth cover is the fraction of measurement intervals, over some arbitrary averaging time, in which clouds are detected. A typical averaging time is 0.5 h.

Other methods are passive, detecting a cloud when sunlight reaching a pyranometer on the ground or on an aircraft is interrupted by cloud shadow (Ek and Mahrt 1991). When the sun is not directly overhead, errors arise because the silhouette of the cloud blocking the sunlight includes the vertical depth of the cloud, not just the horizontal cross-sectional area.

Many observers have used vertically pointing sensors, but little has been mentioned of the accuracy of these measurements. Aviolat et al. (1998) are an exception. They indicate that ceilometers are not a good tool to estimate cloud cover because they are point measurements. The sampling error associated with a point measurement can be large, particularly during periods with low wind speeds, when few clouds move over the sensor. To improve the accuracy of these measurements, a longer averaging time can be used; however, nonsta-

Corresponding author address: Larry K. Berg, Dept. of Earth and Ocean Sciences, The University of British Columbia, 6339 Stores Rd., Vancouver, BC V6T 1Z4, Canada.
E-mail: lkberg@eos.ubc.ca

tionarity of the cloud field could become an important factor. Feijt and van Lammeren (1996) improved their cloud-cover measurements by combining ceilometer measurements with satellite observations.

The purpose of this article is twofold. First, earth-cover errors associated with observations from an upward-looking sensor are compared with averaging time or distance. For airborne sensors, this could be the length of time it takes to fly one flight leg. For sensors on the ground, this corresponds to the length of atmosphere advected over the sensor. Inspired by the work of Poellot and Cox (1977), who looked at the averaging time needed to measure accurate shortwave fluxes, and Santoso and Stull (1999), who designed optimal flight patterns to sample boundary layer turbulence, we conducted tests in which a virtual aircraft is ''flown'' under a simulated cloud field. An empirical set of equations is found for the virtual data that relates the measurement errors to an arbitrary averaging length and earth cover. Second, these virtual results are used to interpret a comparison of passive pyranometer measurements with human estimates of earth cover made during Boundary Layer Experiment 1996 (BLX96; Stull et al. 1997; Berg et al. 1997).

2. Earth-cover observation methods

a. Simulated observations

There has been much debate in the literature about the nature of the spatial distributions of real cumuli. Some researchers have suggested that cumuli are clumped (Plank 1969; Randall and Huffman 1980; Joseph and Cahalan 1990; Sengupta et al. 1990). Other authors believed that fields of cumuli were regular (Bretherton 1987, 1988; Ramirez and Bras 1990). Some authors have assumed that cloud fields were randomly distributed (Ellingson 1982; Zuev et al. 1987). Others have found that smaller cumuli were clumped and the larger cumuli tended to a more regular or random distribution (Weger et al. 1992; Zhu et al. 1992). Ramirez and Bras (1990), Weger et al. (1992), and Zhu et al. (1992) related observed or simulated nearest-neighbor distributions to theoretical nearest-neighbor distributions for a random process, for many different cloud fields. They found that very different looking cloud fields, including random cloud fields, could produce similar nearest-neighbor distributions.

A random cloud field was used in this simulation study. Vertically thin, horizontally circular clouds were randomly placed on a regular 0.1-km grid in a 710 km $\times$ 82 km domain. The clouds were not allowed to overlap, but cloud edges could touch. As judged using standards proposed by Joseph and Cahalan (1990), this simulated cloud field is very slightly regular. Tests showed that cloud-cover statistics generated from slightly regular or completely random cloud fields were indistinguishable from each other.

The cloud diameters were chosen to follow a lognormal distribution. The parameters for the lognormal distribution were chosen to be consistent with the observations of Lopez (1977) and Plank (1969). For the results presented, the mean cloud radius was 0.5 km and the standard deviation was 2.0 km.

Earth-cover values were allowed to range from 5% to 40% for the tests, which corresponds to ''few cumuli'' to ''scattered.'' All of the cloud centers were located within the domain, but clouds could hang off the edge of the domain. This method might lead to inaccurate earth-cover estimates near the edge, because no clouds were allowed to hang onto the domain. To eliminate edge effects, the simulated aircraft ''flew'' horizontal legs within a subdomain of 690 km $\times$ 72 km. Each parallel leg was 0.1 km apart laterally and ranged in length from 5 to 70 km. During each virtual flight, the fraction of the flight leg that was under simulated clouds was recorded to provide a line average. These results also correspond to a cloud field advecting over a ground-based sensor at a variety of wind speeds.

A second experiment using the virtual aircraft was conducted to compare earth-cover estimates made along a single line through the cloud field to the earth cover estimated using a swath (area) average centered on the aircraft. This experiment corresponds more closely to the earth-cover measurements by an observer on an aircraft who can see cloud shadows covering the ground to the left and right of the aircraft track, in addition to the shadows immediately ahead. The width of the swath (3.5 km) was chosen to be similar to the area beneath the aircraft used to estimate earth cover during the field experiment described in the next section.

b. Boundary Layer Experiment 1996 observations

BLX96 was conducted from 15 July to 13 August 1996 over three different regions of Oklahoma and Kansas located within the Atmospheric Radiation Measurement Program Cloud and Radiation Test Bed region (Stokes and Schwartz 1994). The University of Wyoming King Air aircraft flew horizontal legs, each approximately 70 km long, at a number of altitudes in the daytime convective boundary layer. At aircraft speeds of roughly 90 m s^{-1}, each leg took about 15 min to complete. All of the flight legs were flown between 1000 and 1500 LST, with most legs between 1100 and 1400 LST. Solar zenith angles ϕ ranged between approximately 15° and 36° and were less than 30° for 80% of the legs flown.

BLX96 was designed to meet several different goals (Stull et al. 1997). One of these goals was to provide data for verification of boundary layer cumuli parameterizations. Earth cover is a key variable for verification of parameterizations. Standard surface observations are unsatisfactory because they measure sky cover rather than earth cover and would be valid for only a fraction of the flight track. Observations of earth cover by an

observer on the ground (either human or electronic) would be unreliable because only one or two clouds might be directly over the observer, leading to a large sampling error. Satellite observations were not used because many of the small boundary layer cumuli (cumulus humilis) during BLX96 were smaller than weather satellite resolutions.

Because of the shortcomings of these methods, two alternative methods for measuring earth cover were used during BLX96: radiometric and manual. The upward-looking Eppley Laboratory, Inc., Precision Spectral Pyranometer (Model PSP) on the aircraft showed large differences between measurements made inside and outside cloud shadows. A threshold value of 575 W m^{-2} was applied to the unfiltered pyranometer time series to determine when the aircraft passed through a cloud shadow (Ek and Mahrt 1991). The estimated earth cover was defined as the fraction of the whole leg that was within cloud shadows. The pyranometer-measured earth cover was insensitive to the threshold chosen, for thresholds between 375 and 775 W m^{-2}.

The airborne scientist on each flight also made estimates of earth cover based on the cloud shadows projected on the ground. It was fortunate that the area under the flight tracks was divided by roads and fence lines into 800-m (0.5 mi) sections, allowing for more accurate estimates of earth cover. All of the manual estimates for a given flight leg were averaged together to give a leg average. The number of human observations logged during any given leg ranged from 1 to 10. Four different airborne scientists flew during BLX96. Although all four scientists trained together before the field program in an attempt to equalize their observations, there may be biases in earth-cover estimates. Young (1967) found that differences among observers working with the same satellite images were as large as 2 oktas for the range of earth covers he studied. Similar errors might be expected for the observations made during BLX96. The airborne scientists also logged cloud thickness of the cumulus humilis clouds in three ways: 1) by estimating aspect ratio (cloud width to cloud height) visually, 2) by logging cloud-base and cloud-top altitudes during ascent/descent slant aircraft soundings, and 3) via post-flight inspection of footage from the forward-looking automatic airborne video camera.

c. Effect of solar zenith angle on cloud shadows

Using cloud shadows projected on the earth to estimate earth cover is exact only for a ϕ of 0° or, alternatively, for infinitely thin clouds. As ϕ increases, part of the sunlight could be blocked by the cloud sides, causing the shadow projected onto the earth's surface to be larger than the true earth cover. Taller clouds enhance this effect because more sunlight is blocked. For shallow clouds and high sun, however, the earth-cover errors are minimal. During BLX96 most flight legs were flown during fair-weather, anticyclonic conditions within a few hours of solar noon. It was observed during BLX96 that most the cumuli were short, with an aspect ratio between 1 and 2.

A simple analytical experiment can be used to estimate the error in measured earth cover due to different ϕ and cloud aspect ratios. For this analysis, the downwelling radiation is assumed to be plane parallel. Clouds are assumed to have flat bottoms, a square base, and to be semicircular or semielliptical in cross section parallel to the sun's rays (Fig. 1). Clouds are assumed to have a rectangular cross section in the dimension perpendicular to the sun's rays. One important implication of this cloud geometry is that cloud shadow is rectangular.

With these assumptions and a value of ϕ, the amount that cloud shadows overestimate earth cover can be calculated analytically. Figure 1 shows an example in which the cloud shadow is some amount δA larger than the true earth cover A. The geometric location of cloud top is defined using

$$\frac{x^2}{x_c^2} + \frac{z^2}{z_c^2} = 1, \tag{1}$$

where x_c is one-half the cloud width and z_c is the cloud thickness. The location on the cloud at which the sun's ray is tangent to the cloud determines how much radiation the cloud blocks and the size of the cloud shadow ($A + \delta A$). This point is found by taking the derivative of (1) with respect to x to find the slope of the tangent line at any point along the cloud's top. Combining this result with (1) and ϕ yields equations for the z location ($z_{\tan}$) and the x location ($x_{\tan}$) at which the sun's ray is tangent to the cloud's top:

$$z_{\tan} = z_c\left[\frac{x_c^2 \tan^2(\pi/2 - \phi)}{z_c^2} + 1\right]^{-1/2}, \quad \text{and} \tag{2}$$

$$x_{\tan} = x_c[(1 - z_{\tan}^2/z_c^2)]^{1/2}. \tag{3}$$

As shown in Fig. 1, the triangle (ABC) formed by a vertical line through the tangent point, the cloud base, and the line representing the sun's ray can be used to find the length δx added to the cloud shadow. This equation can be written as

$$\delta x = x_{\tan} + z_{\tan}\tan(\phi) - x_c. \tag{4}$$

Equations (3) and (4) show that the error is a function of the cloud thickness, cloud width, and ϕ. As a check of the behavior of these equations we find that, as ϕ approaches 0 in (2), $\tan^2(\pi/2 - \phi)$ approaches infinity and $z_{\tan}$ approaches 0. Using (3), we find that $x_{\tan} = x_c$, and (4) predicts that the error approaches 0, as expected.

The total area of the cloud shadow can be found using (4) and a cloud length of $2y_c$:

$$A + \delta A = 2y_c(2x_c + \delta x) = 4x_c y_c + 2y_c \delta x. \tag{5}$$

The total area is a function of cloud height, cloud diameter, and ϕ. A fractional error can be defined as $[(A + \delta A)/A]$, which, by using (5), can be rewritten as $1 +$

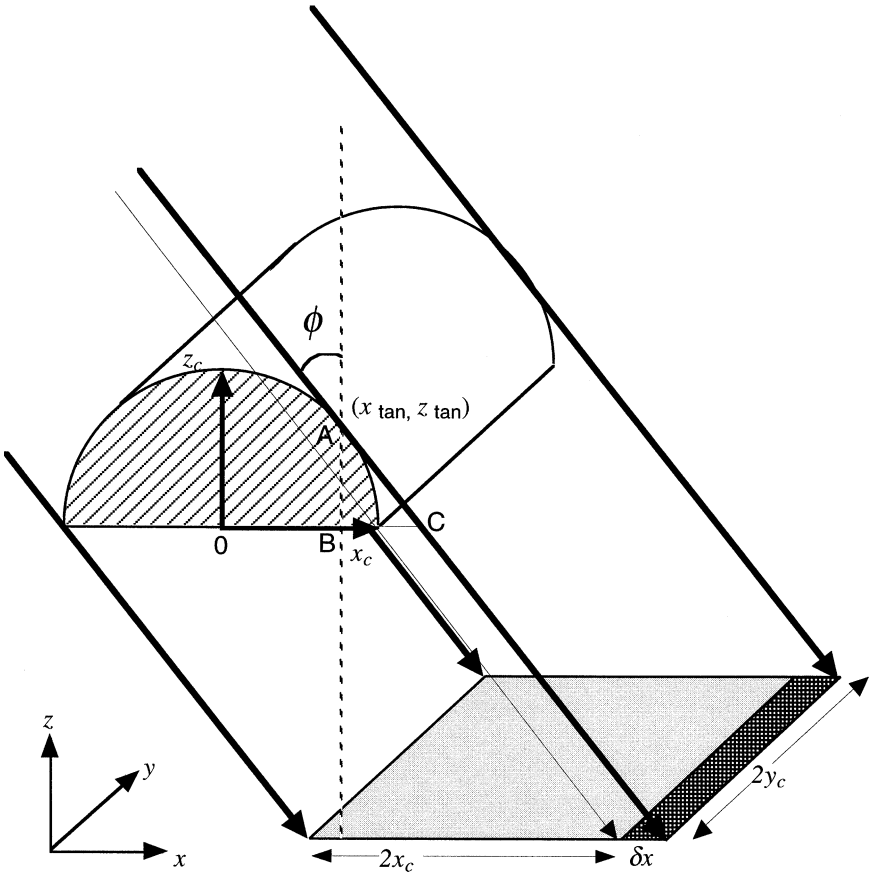

FIG. 1. Sketch showing cloud geometry used to estimate the earth-cover error associated with cloud thickness and solar zenith angle ϕ. Heavy descending arrows represent the actual sun's rays; the thin one represents a ray striking the edge of an infinitely thin cloud. The shaded semicircle aloft is a single boundary layer cumulus with height z_c. The point x_{tan}, z_{tan} marks the tangent point of the sun's ray. Shading below the cloud shows the true cloud width $2x_c$ and the error δx associated with the solar zenith angle.

$\delta x/2x_c$. Combining this form of the fractional error with (2)–(4) yields an equation for the fractional error that is a function of only the aspect ratio of the cloud ($R = 2x_c z_c^{-1}$) and ϕ:

$$\frac{A + \delta A}{A} = \frac{1}{2}\langle 1 + \{1 - [0.25R^2 \tan^2(\pi/2 - \phi) + 1]^{-1}\}^{1/2} + 4R^{-2}[\tan^2(\pi/2 - \phi) + 4R^{-2}]^{-1/2} \tan(\phi)\rangle. \quad (6)$$

From the observations of cloud diameters and cloud heights during BLX96 and from the solar zenith angle calculated from the time, latitude, and longitude of the flights, the error in earth cover associated with the cloud shadows can be calculated. For shallow clouds with an aspect ratio of 2, the fractional error is small, 1.11 for $\phi = 35°$ (Fig. 2). As the clouds grow deeper, the error increases; for clouds with an aspect ratio of 1, the fractional error is 1.36 for $\phi = 35°$ but is much smaller for smaller ϕ. For taller clouds, the error would be even more substantial. Thus, for most of the BLX96 observations the error is small, and the cloud-shadow method can be used to infer earth cover (appendix).

3. Simulated cloud-field results

a. Results

The ''observed'' mean earth cover, estimated by sampling along lines with the virtual aircraft, is very close to the true simulated earth cover based on the known areal coverage of the synthetic clouds (Fig. 3). These results are almost independent of the length of the simulated flight leg, at least for legs as short as 5 km, or about 2–5 times the mean distance to the nearest neighbor, depending on the earth cover. There is a small bias, which increases as the leg length gets shorter (approximately 2% bias for the 5-km-long leg).

The standard deviation of the mean earth cover for all legs can be calculated to give an estimate of likely measurement errors. This leg-to-leg standard deviation decreases with increasing leg length (Fig. 4). The chang-

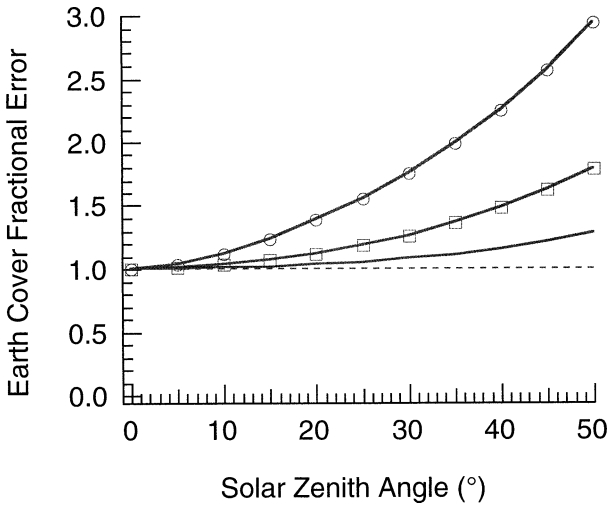

FIG. 2. Solar zenith angle vs earth-cover fractional error for aspect ratios of 2 (no symbol), 1 (squares), and 0.5 (circles). The dashed line marks a fractional error of 1.

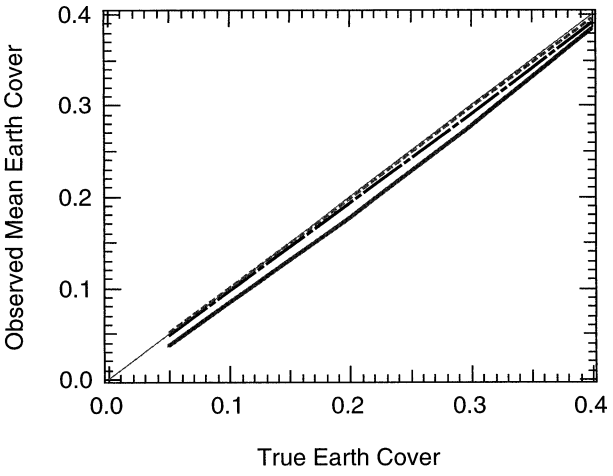

FIG. 3. Mean line-sampled earth cover vs true simulated earth cover for legs of 5- (thick solid), 20- (dot–dashed), and 70-km (dashed) length. The thin solid line is the 1:1 line.

es are smaller for longer legs, however. The standard deviation is smaller for the swath than for the single-line average. Figure 5 provides another, more explicit, look at the differences between the single-line and swath measurements. For this case of 20% true simulated earth cover, the swath estimates of earth cover range from 10% to 33% while the single-line average ranges from about 7% to 42%.

The leg-to-leg standard deviation increases with earth cover for simulated true earth cover values less than about 20% (Fig. 6). For the 5-km-long leg, the standard deviation is larger than the simulated true earth cover for earth covers ranging from 0% to just under 20%. For simulated earth cover greater than 20%, the standard deviation is only a weak function of earth cover. The qualitative shape of the standard deviation curve in Fig. 6 can be explained by the bounded nature of earth cover, which can only range between 0% and 100%. The relatively small leg-to-leg standard deviation ''measured'' by the virtual aircraft at smaller earth covers is affected by the number of legs with no earth cover. For example, given 5-km-long legs and 5% earth cover, over 80% of the legs flown had no earth cover, leading to a smaller standard deviation (although still larger than the observed earth cover) than would be expected if a distribution with negative earth covers was used. As the true earth cover gets larger, there are fewer legs with 0% earth cover, and the standard deviation increases until the effects of the bounding are removed. Similar effects are expected at larger earth covers, because the maximum earth cover is also bounded.

These results have important implications for ground-based instruments. Clouds are advected by the mean wind over ground-based instruments. A hypothetical wind speed of 10 m s^{-1} and an averaging time of 30 min (such as that used by ASOS) corresponds to an averaging length of about 20 km. For legs of this length, the maximum leg-to-leg standard deviation is about 10%, and, for earth covers smaller than about 8%, the standard deviation is larger than the observed earth cover (Fig. 6). To reduce the standard deviation to close to 5%, an averaging time of 90 min is needed. This time period is long; the nonstationarity of the cloud field could be important.

Cases with organized cloud fields have been ignored in this study. The clouds are assumed to be randomly distributed. During periods of strong wind, roll vortices can form (Etling and Brown 1993; Weckwerth et al. 1997). In this case, the clouds would be organized in rows that are nearly parallel to the mean wind. A ground-based sensor might measure earth covers that are very small or very large, depending on the location

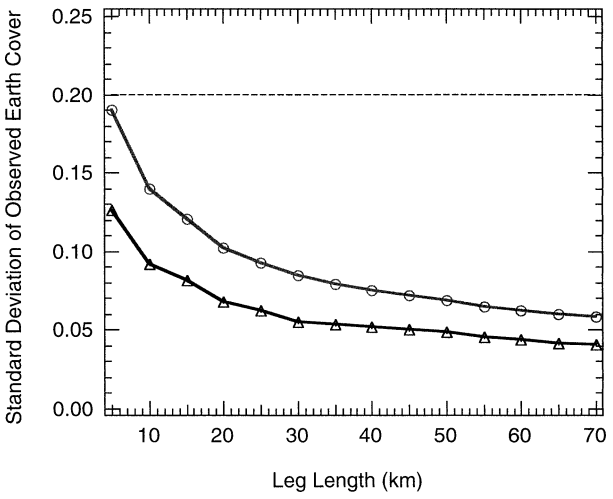

FIG. 4. Leg-to-leg std dev of the observed earth cover vs leg length for single-line averages (circles) and vs leg length for a swath average (triangles) for a case with a true simulated earth cover of 20% (dashed line).

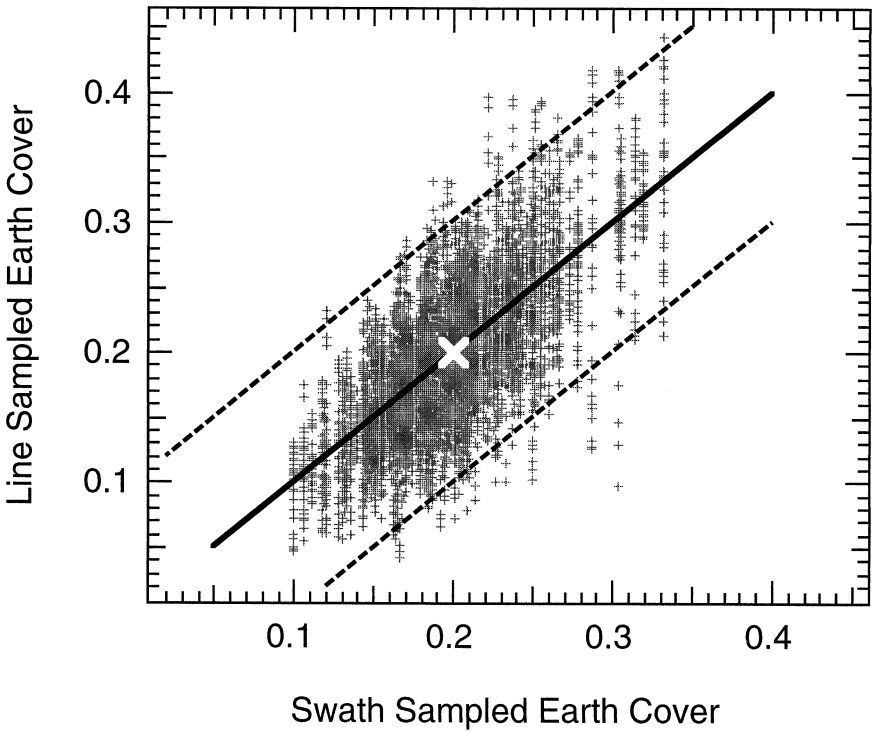

FIG. 5. Simulated line-sampled vs simulated swath-sampled earth cover for a case with a true earth cover of 20% (white X) and a leg length of 70 km. The solid line is the 1:1 line; the dashed lines are ±10% from the 1:1 line.

of the sensor relative to the cloud streets. Thus, the error could be much larger than the values suggested by this study. It is for just this reason that research flights in the real convective boundary layer are usually flown across the wind.

The size distributions of clouds cannot be inferred from a single leg. There were many legs, even at 40% earth cover and for 70-km-long legs, for which the virtual aircraft intercepted only a small number of clouds. When all of the flight legs were combined, however, the cloud size statistics approach the true distribution (not shown).

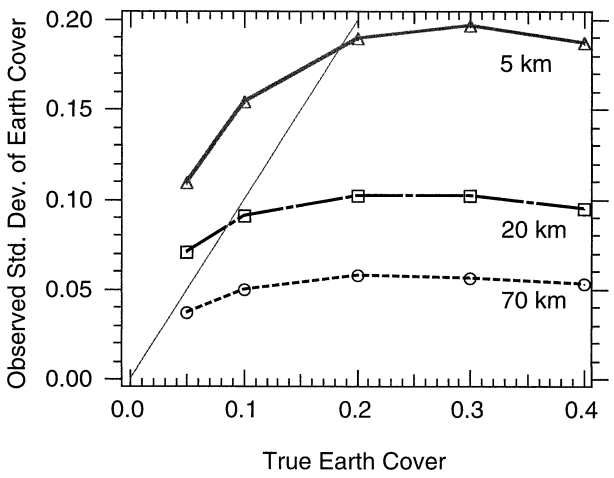

FIG. 6. Leg-to-leg std dev of sample earth cover vs true earth cover for flight legs of 5- (solid line with triangles), 20- (dot–dashed line with squares), and 70-km (dashed with circles) length. The thin solid diagonal line is the 1:1 line, and points above this diagonal line have errors greater than the mean coverage signal.

b. *Applications*

An equation, or a set of equations, that relates the error in the measured earth cover of fair-weather cumuli to the leg length and the earth cover can be found. Such an equation would be useful to scientists planning a field program or interpreting results from previous field work. Figure 4 shows an example of the leg-to-leg standard deviation measured with the virtual aircraft for a true simulated earth cover of 20%. Similar plots were made for a range of simulated earth covers; the general shape of the curves is the same, but there are large differences in the fit parameters. It may be simpler to relate the noise-to-signal ratio (NSR) to the leg length, where NSR is defined to be

$$\mathrm{NSR} = \sigma_x/\overline{x}, \tag{7}$$

where $\overline{x}$ is the average and σ_x is the standard deviation of any variable x. The NSR curves unfortunately also vary greatly with different amounts of earth cover. However, the simulated observations collapse onto one ''universal'' curve when the NSR is normalized by the NSR of the shortest leg flown, which is the maximum NSR

(NSR_{MAX}) observed at a given true simulated earth cover. A power-law relationship was fit to the NSR/NSR_{MAX} points, yielding an expression of the form

$$\frac{NSR}{NSR_{MAX}} = -(0.0832 \pm 0.006) + (2.22 \pm 0.01)l^{-(0.445\pm0.005)}, \quad (8)$$

where l is the averaging length in kilometers. NSR_{MAX} is a function of earth cover (not shown). Again, a power-law relationship was fit to the NSR_{MAX} data, yielding

$$NSR_{MAX} = -(1.03 \pm 0.07) + (0.994 \pm 0.06)\alpha_{cloud}^{-(0.462\pm0.01)}, \quad (9)$$

where α_{cloud} is the earth-cover fraction. Equations (7), (8), and (9) can be combined to give an expression for the leg-to-leg standard deviation given some arbitrary leg length and earth cover:

$$\sigma_{cloud} = \alpha_{cloud}(0.0856 - 0.0827\alpha_{cloud}^{-0.462} - 2.29l^{-0.445} + 2.21\alpha_{cloud}^{-0.462}l^{-0.445}). \quad (10)$$

For leg lengths greater than 15 km, (10) is accurate to within 8% of the standard deviation observed by the virtual aircraft flying under the simulated cloud field. For shorter flight legs, (10) is not as accurate. For example, given 5-km-long legs and 5% earth cover, (10) overestimates the standard deviation observed by the virtual aircraft by about 35% [i.e., 15% predicted by (10) as compared with 11% measured with the virtual aircraft].

As an alternative, when planning a field program, one might be interested in the leg length required to estimate the earth cover to some desired accuracy. Equations (8) and (9) can be manipulated to give

$$l = \left(\frac{NSR}{-2.28 + 2.21\alpha_{cloud}^{-0.462}} + 0.0374\right)^{-2.25}. \quad (11)$$

The average error in leg length predicted by (11) for all simulated earth covers, as compared with the simulated flight legs, is about 3%. The maximum error in leg length estimated using (11) in comparison with observations using the virtual aircraft is 14%, which occurs for a simulated earth cover of 20% [i.e., 60.5 km predicted by (11) as compared with 70 km measured with the virtual aircraft]. In a strict sense, (11) is circular; one must know the earth cover to determine the leg length that is needed to measure the earth cover. In practice, however, a range of applicable earth cover or some approximate value of the earth cover is often known from the climatic data of the field site, so that (11) can be used to estimate the leg lengths needed. For example, during BLX96 all of the flights were to take place during conditions with fair-weather cumuli cover of 0%–30% but not during conditions with more earth cover. So, (11) could be used with hypothetical earth covers ranging from near 0% to as large as 30% to estimate the maximum leg length that would be required to give good earth-cover estimates.

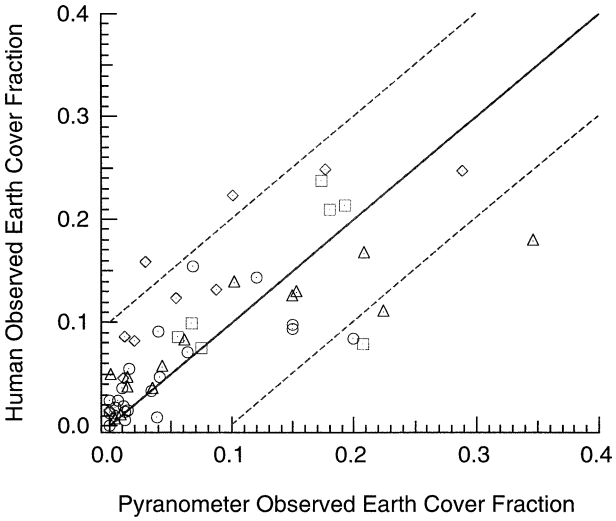

FIG. 7. Human-observed, swath (area) average, earth-cover fraction for each of the four different scientists (different symbols) vs pyranometer-observed, line-sampled, earth-cover fraction for all BLX96 cloudy legs. The thin solid line is the 1:1 line; the thin dashed lines are ±0.1 from the 1:1 line.

How does the leg length required for accurate estimates of earth cover compare to the leg lengths needed for accurate measurements of turbulent statistics? Lenschow et al. (1994) found that, for a leg length of 20 km, the random error in the scalar fluxes is about 18%. For a leg length of 70 km, the error in the scalar fluxes drops to about 12%. From the Lenschow et al. work, the requirements for the accurate measurement of turbulent quantities in the boundary layer are more strict than that required for measurements of earth cover. Thus, choosing a leg length to give accurate turbulent statistics should meet the requirements needed for accurate measurement of fair-weather boundary layer earth cover.

4. Observed BLX96 results

The agreement between the airborne observer and the aircraft-mounted pyranometer during BLX96 is good but not perfect (Fig. 7). These observations have been corrected for the cloud-shadow error using (6). Most of the observations (90%) are within ±10% of each other. There apparently is little bias among the different observers. When the earth cover is small, the airborne observer tended to estimate larger amounts of earth cover than was recorded by the pyranometer.

A straight line can be fit to the observations. The errors in the pyranometer and the errors in the human observations must both be accounted for when fitting a straight line to the data (Press et al. 1992). The error in the aircraft pyranometer was assumed to follow (10) using a 70-km-long leg. The human errors were taken

to be similar to those suggested by Young (1967). Two factors should be considered when using Young's error analysis. His data were for humans analyzing satellite photos rather than taking a quick look at a real cloud field, so the errors in BLX96 are likely to be larger than those found by Young. The smallest earth cover he used was about 3 oktas. This value is about the maximum earth cover observed during BLX96. Young found that the error in measured earth cover shrinks as the true earth cover increases. He argues that as the true earth cover shrinks, the error in measured earth cover shrinks as well. He suggests that for an earth cover of 0, there would be 0 error in the human observations. This assumption precludes using some of the BLX96 data in the prescribed fitting procedure because 0 error leads to a singularity in the calculations. With all human observations of 0 earth cover removed, the calculated slope of the best-fit line is 0.9 ± 0.13 and the intercept is 0.0004 ± 0.0002. These fit parameters indicate that the two observed distributions are drawn from the same parent distribution.

A second test, the Kolmogorov–Smirnov test, can be used to determine if the observed distributions came from the same parent distribution (Press et al. 1992). This test compares the cumulative distributions of two variables. The largest value of the difference between these two distributions is used as a test statistic and is compared with the Kolmogorov–Smirnov probability function to determine the confidence of the estimate. For the BLX96 data, the largest difference in the cumulative distribution functions was 0.18 and the p value was 0.24, so there is insufficient evidence to indicate that the distributions are different.

While the statistical tests suggest that the parent distributions are the same, there are a number of reasons for the scatter in the figure. Sampling errors are a likely explanation. The airborne observer looked at cloud shadows projected within a swath area on the ground under the aircraft. When averaged over the entire flight leg, this corresponds to a wide swath, approximately 3.5 km wide during BLX96, through the cloud field. The pyranometer is a line estimate through the cloud field. The two methods are sampling different areas to estimate the earth cover. The experiment with the virtual aircraft can also provide insight into this question. Although constructed using only one true simulated earth cover of 20%, Fig. 5 is illuminating. Points for cases of different simulated earth cover could be added to the plot, but the qualitative results would be unchanged. Many of the differences between the swath-based and the line-sampled earth cover in Fig. 5 are similar in magnitude to the differences shown in Fig. 7. Henderson-Sellers and McGuffie's (1990) results are similar. They compared sky cover and earth cover measured from all-sky images and had much scatter. They found many cases in which there were not clouds directly above the sensor although some clouds were reported nearby, similar to the BLX96 results at small earth cover.

Another factor that could contribute to the differences at smaller earth cover is the method used by the airborne observer to measure earth cover. During most of the flights with clouds, it was usual for earth cover to vary along any single 70-km leg as the aircraft flew through meso-γ-scale regions that were relatively clearer or cloudier than others. For these situations, the observer only reported the earth cover at the start of each leg and again when they noticed a change during the flight. Also, at other times, the observer was busy with other duties. So, particularly when the earth cover is small, there are portions of the leg having no earth cover that might not be accurately reported. If some 0 values were missed, then the leg average would be too large.

5. Conclusions

The primary goal of this work was to determine the accuracy of earth-cover measurements by both ground-based and aircraft-mounted sensors for a range of boundary layer earth covers. Two different comparisons were made. First, sampled results for both line and swath averages were compared with the prescribed cloud cover from a simulated cloud field. These results suggested that, for short flight legs or averaging times, the observed standard deviation was often larger than the mean earth cover. When longer flight legs or averaging times were used, the earth-cover measurements were within $\pm 5\%$ of the true cover for a wide range of earth cover.

Using the virtual data, a set of empirical equations was presented so that the appropriate leg length could be found for some arbitrary NSR and to find standard deviation of earth cover from leg length and true earth cover. The accuracy of earth cover inferred from ceilometer or other vertically pointed instruments depends on a number of factors, including wind speed. At high wind speeds, these measurements might be suspect because of horizontal roll vortices; at lower wind speeds, the measurements are suspect because of random sampling errors.

For shallow boundary layer cumuli (i.e., cumulus humilis) and high sun angle it was shown that the shading of the ground by the vertical portion of the cloud silhouette caused errors of about 5%. For true earth coverage between 5% and 30%, this vertical silhouette error was small in comparison with typical observation and sampling errors of about 17% for 5-km-long legs and was about the same size as the observation and sampling errors for 70-km-long legs.

Second, estimates of earth cover from an aircraft-mounted pyranometer were compared with estimates from an airborne observer. In general, there was good agreement between the airborne human observer and the pyranometer-measured earth cover from BLX96. Tests were conducted that suggest that the two observed distributions came from the same parent distribution. However, it also seems that the human observer tends to estimate a larger earth cover at small values of earth

cover. Two suggestions are made that might explain these differences: 1) different sampling techniques between the human and pyranometer and 2) improper recording of 0% earth cover.

Field work should include a structured methodology for the airborne observer to measure earth cover. It is recommended that human estimates should be made at regular intervals during the flight and intercomparisons among the observers should be undertaken. This research also shows, however, that given the accuracy of the pyranometer-measured earth cover for long flight legs, human estimates might not be necessary.

Acknowledgments. The lead author was funded by a University of British Columbia University Graduate Fellowship and by the Canadian Climate Research Network through grants from the National Science and Engineering Research Council (NSERC), Meteorological Service of Canada (MSC), and the Canadian Foundation for Climate and Atmospheric Science. Additional support was provided by the Geophysical Disaster Computational Fluid Dynamics Centre and grants from NSERC and Environment Canada. The BLX96 field program was funded by the U.S. National Science Foundation (NSF) under Grant ATM-9411467. E. Santoso and J. Hacker are thanked for their work as airborne scientists during BLX96. The staff and flight crew of the University of Wyoming King Air aircraft (sponsored by NSF) helped to make BLX96 a success. Suggestions provided by two anonymous reviewers greatly improved this article.

APPENDIX

BLX96 Cloud-Field Statistics

Table A1 provides the descriptive material for all cloudy days during BLX96.

TABLE A1. Date, time, solar zenith angle, cloud-base height, cloud-top height, and boundary layer cloud type [either Cumulus (Cu) humilis or Cu mediocris] of all BLX96 cloudy days.

Date	Leg	Time (LST)	Time (UTC)	Solar zenith angle (°)	Cloud-base height (m)	Cloud-top height (m)	Boundary layer cloud type
15 Jul	1	10.2	16.2	32.7	1552	1825	Cu humilis
	2	11.4	17.4	20.7	1654	2343	Cu humilis
	3	11.6	17.6	18.7	1675	2452	Cu mediocris/Cu humilis
	4	11.9	17.9	17.0	1697	2565	Cu mediocris/Cu humilis
	5	13.2	19.2	18.2	1872	2704	Cu humilis
	6	13.4	19.4	20.1	1906	2731	Cu humilis
	7	13.7	19.7	22.3	1939	2758	Cu humilis
16 Jul	1	10.8	16.8	26.2	973	1626	Cu humilis
	2	11.9	17.9	15.5	1142	2039	Cu humilis
	3	12.2	18.2	14.5	1177	2124	Cu humilis
	4	12.4	18.4	14.1	1213	2213	Cu humilis
	5	13.7	19.7	21.2	1195	1926	Cu humilis
	6	13.9	19.9	23.7	1192	1870	Cu humilis
	7	14.1	20.1	26.1	1188	1816	Cu humilis
23 Jul	1	11.8	17.8	19.1	804	1197	Cu humilis
	2	12.9	18.9	17.0	802	1081	Cu humilis
	3	14.1	20.1	26.1	1347	1576	Cu humilis
	4	14.3	20.3	28.9	1467	1684	Cu humilis
	5	14.6	20.6	31.9	1592	1798	Cu humilis
25 Jul	1	11.1	17.1	24.7	1733	1965	Cu humilis
	2	12.3	18.3	17.4	2253	2588	Cu humilis
	3	12.6	18.6	17.4	2364	2720	Cu humilis
	4	12.8	18.8	18.1	2467	2844	Cu humilis
	5	14.1	20.1	27.8	2441	2664	Cu humilis
	6	14.3	20.3	30.4	2436	2629	Cu humilis
	7	14.6	20.6	33.3	2430	2590	Cu humilis
27 Jul	1	11.0	17.0	26.6	551	696	Cu humilis
	2	12.2	18.2	17.8	768	932	Cu mediocris/Cu humilis
	3	12.5	18.5	17.3	818	986	Cu humilis
	4	12.7	18.7	17.4	866	1038	Cu mediocris/Cu humilis
	5	13.9	19.9	25.3	944	1126	Cu humilis
	6	14.2	20.2	28.0	962	1146	Cu humilis
	7	14.5	20.5	31.0	979	1166	Cu humilis
28 Jul	1	11.3	17.3	22.1	941	1556	Cu mediocris/Cu humilis
	2	12.5	18.5	16.5	1164	1782	Cu mediocris/Cu humilis
	3	12.8	18.8	17.2	1217	1836	Cu mediocris/Cu humilis
	4	13.1	19.1	18.6	1266	1886	Cu mediocris/Cu humilis
	5	14.3	20.3	29.8	1305	1600	Cu mediocris/Cu humilis
	6	14.6	20.6	33.1	1314	1532	Cu humilis
	7	14.9	20.9	36.3	1323	1468	Cu humilis

TABLE A1. (*Continued*)

Date	Leg	Time (LST)	Time (UTC)	Solar zenith angle (°)	Cloud-base height (m)	Cloud-top height (m)	Boundary layer cloud type
31 Jul	1	11.2	17.2	24.6	1542	1631	Cu humilis
	2	12.4	18.4	18.7	1720	1991	Cu humilis
	3	12.7	18.7	19.1	1762	2076	Cu humilis
	4	13.0	19.0	20.2	1804	2160	Cu humilis
	5	14.2	20.2	29.6	1938	2435	Cu humilis
	6	14.5	20.5	32.6	1971	2504	Cu humilis
	7	14.7	20.7	35.6	2003	2569	Cu humilis
2 Aug	1	11.0	17.0	26.1	838	996	Cu humilis
	2	12.2	18.2	18.0	920	1231	Cu humilis
	3	12.5	18.5	17.7	938	1284	Cu humilis
	4	12.7	18.7	18.1	957	1339	Cu humilis
	5	14.0	20.0	26.7	1049	1305	Cu humilis
	6	14.2	20.2	29.5	1069	1297	Cu humilis
	7	14.5	20.5	32.7	1091	1289	Cu humilis

REFERENCES

Appleman, H. S., 1962: A comparison of simultaneous aircraft and surface cloud observations. *J. Appl. Meteor.*, **1,** 548–551.

ASOS Program, 1998: ASOS user's guide. 70 pp. [Available online at http://www.nws.noaa.gov/asos/.]

Aviolat, F., T. Cornu, and D. Cattani, 1998: Automatic clouds observation improved by an artificial neural network. *J. Atmos. Oceanic Technol.,* **15,** 114–126.

Berg, L. K., R. B. Stull., E. Santoso, and J. P. Hacker, 1997: Boundary Layer Experiment 1996 airborne scientist flight log. Boundary Layer Tech. Rep. 97-1, 116 pp. [Available from Prof. R. Stull, Atmospheric Science Programme, Dept. of Earth and Ocean Sciences, UBC, 6339 Stores Rd., Vancouver, BC V6T 1Z4, Canada.]

Bretherton, C. S., 1987: A theory for nonprecipitating moist convection between two parallel plates. Part I: Thermodynamics and ''linear'' solutions. *J. Atmos. Sci.*, **44,** 1809–1827.

——, 1988: A theory for nonprecipitating convection between two parallel plates. Part II: Nonlinear theory and cloud field organization. *J. Atmos. Sci.*, **45,** 2391–2415.

——, E. Klinker, A. K. Betts, and J. A. Coakley Jr., 1995: Comparison of ceilometer, satellite, and synoptic measurements of boundary-layer cloudiness and the ECMWF diagnostic cloud parameterization scheme during ASTEX. *J. Atmos. Sci.*, **52,** 2736–2751.

Ek, M., and L. Mahrt, 1991: A formulation for boundary-layer cloud cover. *Ann. Geophys.*, **9,** 716–724.

Ellingson, R. G., 1982: On the effects of cumulus dimensions on longwave irradiance and heating rate calculations. *J. Atmos. Sci.*, **39,** 886–896.

Etling, D., and R. A. Brown, 1993: Roll vortices in the planetary boundary-layer—a review. *Bound.-Layer Meteor.*, **65,** 215–248.

Fairall, C. W., A. B. White, J. B. Edson, and J. E. Hare, 1997: Integrated shipboard measurements of the marine boundary layer. *J. Atmos. Oceanic Technol.*, **14,** 338–359.

Feijt, A., and A. van Lammeren, 1996: Ground-based and satellite observations of cloud fields in the Netherlands. *Mon. Wea. Rev.*, **124,** 1914–1923.

Grimsdell, A. W., and W. M. Angevine, 1998: Convective boundary layer height measurement with wind profilers and comparison to cloud base. *J. Atmos. Oceanic Technol.*, **15,** 1331–1338.

Henderson-Sellers, A., and K. McGuffie, 1990: Are cloud amounts estimated from satellite sensor and conventional surface-based observations related? *Int. J. Remote Sens.*, **11,** 543–550.

Hoyt, D. V., 1977: Percent of possible sunshine and the total cloud cover. *Mon. Wea. Rev.*, **105,** 648–652.

Joseph, J., and R. F. Cahalan, 1990: Nearest neighbor spacing of fair weather cumulus clouds. *J. Appl. Meteor.*, **29,** 793–805.

Lazarus, S. M., S. K. Krueger, and G. G. Mace, 2000: A cloud climatology of the southern Great Plains ARM CART. *J. Climate,* **13,** 1762–1775.

Lenschow, D. H., J. Mann, and L. Kristensen, 1994: How long is long enough when measuring fluxes and other turbulence statistics? *J. Atmos. Oceanic Technol.*, **11,** 661–673.

Lopez, R. E., 1977: The lognormal distribution of cumulus cloud populations. *Mon. Wea. Rev.*, **105,** 865–872.

Malick, J. D., J. H. Allen, and S. Zakanycz, 1979: Calibrated analytical modeling of cloud-free intervals. *Proc. Soc. Photo-Opt. Instrum. Eng.*, **195,** 142–147.

Plank, V. G., 1969: The size distribution of cumulus clouds in representative Florida populations. *J. Appl. Meteor.*, **8,** 46–67.

Poellot, M. R., and S. K. Cox, 1977: Computer simulation of irradiance measurements from aircraft. *J. Appl. Meteor.*, **16,** 167–171.

Press, W. H., S. A. Teukolsky, W. T. Vetterling, and B. P. Flannery, 1992: *Numerical Recipes in C: The Art of Scientific Computing.* Cambridge University Press, 994 pp.

Ramirez, J. A., and R. L. Bras, 1990: Clustered or regular cumulus cloud fields: The statistical character of observed and simulated cloud fields. *J. Geophys. Res.*, **95,** 2035–2045.

Randall, D. A., and G. J. Huffman, 1980: A stochastic model of cumulus clumping. *J. Atmos. Sci.*, **37,** 2068–2078.

Santoso, E., and R. B. Stull, 1999: Use of synthetic data to test flight patterns for a boundary layer field experiment. *J. Atmos. Oceanic Technol.*, **16,** 1157–1171.

Sengupta, S. K., R. M. Welch, M. S. Navar, T. A. Berendes, and D. W. Chen, 1990: Cumulus cloud field morphology and spatial patterns derived from high spatial resolution Landsat imagery. *J. Appl. Meteor.*, **29,** 1245–1267.

Stokes, G. M., and S. E. Schwartz, 1994: The Atmospheric Radiation Measurement (ARM) Program: Programmatic background and design of the Cloud and Radiation Test Bed. *Bull. Amer. Meteor. Soc.*, **75,** 1201–1221.

Stull, R., E. Santoso, L. Berg, and J. Hacker, 1997: Boundary Layer Experiment 1996 (BLX96). *Bull. Amer. Meteor. Soc.*, **78,** 1149–1158.

Weckwerth, T. M., J. W. Wilson, R. M. Wakimoto, and N. A. Crook, 1997: Horizontal convective rolls: Determining the environmental conditions supporting their existence and characteristics. *Mon. Wea. Rev.*, **125,** 505–526.

Weger, R. C., J. Lee, T. Zhu, and R. M. Welch, 1992: Clustering, randomness and regularity in cloud fields: 1. Theoretical considerations. *J. Geophys. Res.*, **97,** 20 519–20 536.

White, A. B., C. W. Fairall, and J. B. Snider, 1995: Surface-based

remote sensing of marine boundary-layer cloud properties. *J. Atmos. Sci.*, **52,** 2827–2838.
Young, M. J., 1967: Variability in estimating total cloud cover from satellite pictures. *J. Appl. Meteor.*, **6,** 573–579.
Zhu, T., J. Lee, R. C. Weger, and R. M. Welch, 1992: Clustering, randomness, and regularity in cloud fields: 2. Cumulus cloud fields. *J. Geophys. Res.*, **97,** 20 537–20 558.
Zuev, V. E., R. B. Zhuravleva, and G. A. Titov, 1987: Modeling of outgoing longwave radiation in the presence of broken clouds. *J. Geophys. Res.*, **92,** 5533–5539.